An Unusually High Summertime Wave Flight

Edward E. (Ward) Hindman
Earth and Atmospheric Sciences Department and the National Oceanic and Atmospheric Administration
Cooperative Remote Sensing Science and Technology Center
The City College of New York, NYC, NY 10031 USA, hindman@sci.ccny.cuny.edu

Ray L. McAnelly and William R. Cotton
Atmospheric Science Department, Colorado State University,
Ft. Collins, CO 80524 USA, raymc@atmos.colostate.edu

Todd Pattist
50 Harvest Wood Road, Rockfall, CT 06481 USA, pattist@snet.net

and

Richard M. Worthington
Physics Department, University of Wales, Aberystwyth, SY23 3BZ, Wales, rrw@aber.ac.uk

XXVII OSTIV Congress, Leszno, Poland, 2003

Abstract

One of the highest wave flights ever achieved over the Catskill Mountains of southern New York State USA occurred surprisingly on 5 July 2002 (17,990 ft, 5485 m MSL). Using observed meteorological conditions with numerical-simulation models, most features of the wave were reproduced. Using the simulations, it appears the flight could have gone much higher had IFR clearance been obtained. This extraordinary mountain wave appears to have been enhanced by convective activity within the boundary layer above the Catskill Mountains.

Introduction

When forced over a mountain range, high-speed, stable air will develop a series of vertical undulations downwind known as lee-waves. If the air is sufficiently moist, standing-lenticular clouds will form at the crests of the waves. Lee-waves are best developed during the mid-latitude winter and spring because of the strong polar front jet-stream. The jet-stream is weaker during the summer months due to the smaller N-S temperature gradient. Thus, the wave flight described here is remarkable because it occurred during the summertime and was one of the highest wave flights ever flown from the Wurtsboro, New York USA airport (41.60N, 74.46W) where regular glider operations began in the 1940s[1].

On 5 July 2002 at 1527 EST (2027UTC), the fourth author flying his 16.6m Ventus sailplane (WH) reached an altitude of 17,990 feet MSL (5483m) in wave over the Catskill Mountains of southern New York State. WH could have climbed higher at the location (41.538N, 74.284W) but was not cleared for IFR flight. A number of sailplane pilots contacted the wave that afternoon, but none were as successful as Pattist. For example, the first author reached 11,500 ft MSL.

The purpose of this paper is to explain the meteorological conditions during the flight of WH using surface, upper-air and satellite images. Further, numerical simulation models were used to diagnose the air motions and cloud patterns during the wave flight. According to these results, it appears WH may have been able to climb much higher had clearance been obtained.

Flight data

The Global Positioning System (GPS) flight track of WH is illustrated in Fig. 1. (Figures begin on pg.12) The track changes colors to indicate altitude: the warm colors are low altitudes (500 ft MSL) while the cold colors are high altitudes (18,000 ft MSL). The takeoff was from Wurtsboro Airport at 1140 EST (1640 UTC). Using thermals, WH worked slowly NE along the Shawangunk Ridge in the strong NW flow. Cloud base (5,700 ft MSL) was reached SW of the Ellenville Airport.

There, WH contacted the wave (referred to as the *First wave region*). WH climbed to a little over 8000 ft MSL in this area. Thereafter, WH penetrated NNE toward Piolis Airport and contacted an even stronger wave component WSW of the airport (*Second wave region*). At that location, the flight track turns sharply from green to blue indicating a significant gain in altitude. WH continued to climb in wave over and NW of the airport (*Third wave region*). Finally, WH turned NW and penetrated to another upwind component and climbed to the maximum altitude (*Fourth wave region*). This area has the darkest blue colors on the track.

The barogram trace of WH is illustrated in Fig. 2. The climbs of WH in the four wave regions occurred as follows: (1) 17:27 to 17:45 UTC (5,000 to 8,200 ft MSL), (2) 18:00 to 18:50 UTC (6,900 to 13,300 ft MSL), (3) 18:53 to 19:12 UTC (12,500 to 15,500 ft MSL), (4) 19:16 to 20:10 UTC (13,700 to 17,990 ft MSL).

Figure 3 shows the variometer values and the corresponding GPS ground speed of WH. Referring to the upper variometer plot, when climbing in the wave, WH was flown at a glider speed

that produced a sink rate of about 0.6 m/s. Note the fluctuations in the climb rate over short time scales throughout the flight. Some of that is likely due to glider maneuvering, but a lot of it is really in the wave. Pattist constantly marked out the best wave spots, flew through them, watching the variometer drop, returned to them, etc. The best estimate of the vertical wind speed is the value from the plot plus 0.6 m/s, except in those regions where WH is clearly running to a new spot. Since WH did not circle in wave, a good estimate of horizontal wind speed could not be obtained. Without the horizontal wind speed, the airspeed could not be obtained or the polar sink rate needed to correct the vertical wind speed.

Now, refer to the lower ground speed plot in Fig. 3. In thermals and in wave, the airspeed of WH was fairly constant when climbing. In thermals, the horizontal wind speed and direction was determined from drift. In wave, sometimes WH would be headed upwind, sometimes downwind, sometimes in-between, thus, it was not possible to determine the wind direction. But, the maximum ground speed minus the minimum ground speed should equal approximately twice the wind speed. It can be seen that from 17:20 to about 18:40 UTC the peaks are roughly the same maximum height and the valleys are about the same minimum height, within 2-3 m/s. The envelope of the speed variation was constructed and divided by 2, to obtain the approximate wind speed. The speed seems to be fairly constant until 18:40 UTC. Then, an increase is seen in the envelope dimension, signaling a wind speed increase at around 13,000 ft MSL. Presumably this is due to faster moving air aloft, but it could be a simple wind speed change at all altitudes. Note another characteristic that changed at 18:40. The high-speed peaks (headed downwind with wind added to airspeed) are much farther apart and are separated by longer periods of slower ground speeds. This is characteristic of the typical wave flying technique. As the wind speed increases, more time is spent headed upwind (slow ground speed). Only occasionally are downwind turns made and, then, only briefly to remain in the rising part of the wave.

Using the methods described above, wind speeds and directions were estimated from the flight track data. The results are displayed in Table 1 (pg. 23).

Meteorology

Surface

The surface weather maps that bound the flight of WH are shown in Fig. 4. It can be seen that a cold front passed Wurtsboro Airport overnight and a clear, NW flow was well established by the morning of 5 July. Light precipitation occurred at higher elevations upwind of Wurtsboro at 0700 EST but vanished as the air sank toward Wurtsboro.

Upper-air

The atmospheric soundings upwind and downwind of the Catskill Mountains during the flight are displayed in Fig. 5. The soundings exhibit the characteristics associated with trapped-lee waves as described by Durran[2]. First, the temperature distribution reveals a convectively mixed layer (surface to 850 mb) with a stable layer above (increasing potential temperature with height). Second, low-speed winds occurred in the mixed layer and speeds increased with height in the stable layer. These conditions imply a discontinuous two-layer structure for the Scorer parameter, smaller values in the mixed layer and larger values in the stable layer.

The estimated wind speeds and directions from the flight track (Table 1) compare favorably with the winds from the soundings in the convective boundary layer (surface to 850 mb). In the region of wave above, the estimated wind speeds are less than the sounding winds.

Satellite

The 5 July 2002, 2225 UTC (1725 EST) NOAA-14 visible image is displayed in Fig. 6. The large yellow circle surrounds 42.2N, 74.5W and the N-S oriented Hudson River can be seen in the lower right of the image. The track of WH is superimposed on the image. Cloud streets (aligned NW - SE) can be seen to the west of the yellow circle where it is sunnier (more hours before sunset) and the trapped lee-wave clouds (aligned SW-NE) were to the east of the circle beyond the edges of the figure. There appears to be a mixture of both in the center of the picture, sort of a "checkerboard" pattern. This is in the region where WH reached the maximum altitude.

This "checkerboard" cloud pattern has been identified by Worthington[4] as mountain waves launched by convective activity within the boundary layer above mountains. A 3D schematic of the pattern appears in Bradbury[5]. Applying that schematic to the 5 July case, the NW-SE cumulus cloud streets and convective rolls are within the convective boundary layer and the wave clouds are in the stable air above with their lines of constant phase at right angles to the cumulus streets below. The convective activity apparently enhanced the lee-waves leading to the extraordinary altitude achieved by WH.

The visible and infrared images during the flight of WH from the GOES-East are displayed in Fig. 7. It can be seen the trapped lee-wave clouds visible in Fig. 6 advance on WH during the period as do some thin, bright wave clouds apparent in the infrared images. The tops of the lee-wave clouds are 6C or about 700 mb while the wave clouds are at -27C which is above 400 mb. The "checkerboard" cloud pattern apparent in Fig. 6 began to appear in the SW portion of the 2002 UTC GOES image.

Modeling

1-D

The atmospheric sounding analyses program RAOB[6] contains an algorithm for determining the maximum vertical displacement and wavelength of an air parcel flowing through a mountain lee-wave. The critical factor in the algorithm is the Lyra-Scorer parameter (LSp, m^{-2}) which is a function of atmospheric stability and vertical wind shear. When the LSp decreases with increasing height, the conditions are favorable for trapped lee-wave development. The following mountain parameters determine the wave characteristics: height of the mountain barrier above the upwind sounding station, the distance between the mountain ridge (center-line) and windward slope as measured at the mid-elevation of the ridge and the angle of the wind impacting the ridge.

The initial conditions to the RAOB algorithm consisted of the mountain parameters and an upwind sounding. The upwind sounding is displayed in Fig. 5. The sounding location is near Oneonta, NY on the plains upwind of the Catskill Mountains.

Oneonta is at an elevation of 1,100 feet MSL and the highest ridges of the Catskills are approximately 3,600 feet MSL along the eastern escarpment that borders the Hudson River Valley. These elevation values produce a ridge height of 2,500 feet. The Catskills are a series of ridges beginning just east of Oneonta and extending approximately 55 nautical miles to the SE culminating at the eastern escarpment. Thus, the ridge half-width was assigned a value of 25 nautical miles. The sounding location was chosen so the winds were perpendicular to the ridge (0 degree orientation).

These initial conditions produced no wave. So, the half-width was reduced to the dimensions of just the eastern escarpment ridge, about 2 nautical miles (nm). Two waves were predicted one at 3,660 m MSL (12,005 ft MSL) with a wavelength of 4.3 nm and a maximum vertical speed of 190 fpm and the other between 5,730 and 5,781 m MSL (18,794 to 18,962 ft MSL) with a wavelength of 6-9 nm and a maximum vertical speed of 243 to 422 fpm.

To predict the maximum potential wave amplitude following Corby and Wallington[7], the default conditions were chosen: 1 km-high ridge with a half-width adjusted to the natural wavelength of the air stream. This increased ridge height is consistent with the depth of the convective-boundry layer over the mountains revealed by the more detailed numerical simulations in the next section. These conditions produced three regions of wave: the first between 2,000 and 2,500 m MSL with a wavelength of 2.5 nmi and a maximum vertical speed of 477 fpm, the second 3,660 m MSL with a wavelength of 4.3 nmi and a maximum vertical speed of 618 fpm and the third between 5,040 and 5,781 m MSL with a 4 to 8 nmi wavelength and a maximum vertical speed of 500 to 600 fpm.

These results are consistent with the 2nd, 3rd and 4th wave regions encountered by WH but did not reproduce the 1st wave region (Table 1).

In an attempt to simulate the 1st wave region, the significant ridge SE of the Ellenville Airport was inserted into the RAOB two-mountain simulation. A second ridge was inserted 15 nm downwind of the main ridge with the following characteristics: a height of 2,000 ft AGL, 15 nm separated the ridges, the ridge half-width was 2 nm and the wind was perpendicular to the ridge. This simulation did not change the results from the previously performed prediction.

RAMS at CSU

To investigate the atmospheric structure of the wave event in greater detail, a high-resolution, three-dimensional simulation was performed using Version 4.29 of the Regional Atmospheric Modeling System (RAMS) at Colorado State University (CSU). RAMS is a state-of-the-art, primitive-equation model with sophisticated parameterizations for radiation, microphysics, land/atmospheric interactions and sub-grid scale convection and mixing (Cotton, et al.[8]).

The simulation was configured similar to the real-time RAMS forecast simulations that have been run once or twice daily at CSU for many years (e.g., Cotton, et al.[9]); see "realtime forecasts" at rams.atmos.colostate.edu/realtime/). Two-way interactive grid nesting was utilized, with a parent grid (Grid 1) covering the northeastern U.S. and southeastern Canada at 32 km horizontal

grid-point spacing. Grids 2, 3 and 4 were successively nested down to the region of interest with a grid-point spacing of 8 km, 2 km, and 0.5 km, respectively (Fig. 9 illustrates Grids 3 and 4). The finest grid encompasses the entire Catskill Mountain range and resolves its topography well. A terrain-following vertical coordinate system had vertical spacing beginning at 100 m at the surface and gradually stretched to a constant 500 m spacing above 4000 m MSL. The model top extended to 17 km MSL, well into the stratosphere.

The RAMS simulation was initialized at 1200 UTC on 5 July 2002 and integrated for 12 hours to 0000 UTC on 6 July. The 12-hour simulation required 13 hours of computer time on the CSU Linux-based PC-cluster with 22 to 24 parallel processors (the extremely high resolution Grid 4 resulted in a model setup that is significantly more computationally intensive than the standard 3-grid setup for the realtime forecast simulations which take 5 hours to produce a 48-hour forecast). The initial conditions were based on the National Center for Environmental Prediction's (NCEP's) operational Eta model forecast cycle initialized at 1200 UTC on 5 July 2002. The Eta initialization data, available at 80 km horizontal grid spacing and at 50 mb vertical spacing, were interpolated onto the RAMS grids. Time dependent lateral and top boundary conditions utilized the 6-hour and 12-hour forecasts from that operational Eta run. Output files for analysis of the RAMS simulation were saved at 15min intervals. The simulation will be displayed and discussed, first, in the plan view and, then, in the vertical cross-section view.

Plan views of the simulation

The vertical air motions that produced the "checkerboard" cloud pattern revealed in Figs. 6 and 7 were reproduced in the simulation as shown on Grid 3 at the 850 mb level at 1730 UTC (Fig. 10). Also, the cloud pattern was reproduced in the corresponding simulated relative humidity field on Grid 4 at the 850 mb level (Fig. 11). The boundary-layer (BL) rolls are seen in Figure 10 aligned NW-SE and the superimposed gravity waves are oriented SW-NE. The BL rolls began to appear in the simulation at 1615 UTC and were weakening by 2100 UTC. In animation, the long, sinuous rolls appeared to move back and forth like "worms". For the most part, the BL rolls were best defined on Grid 4 suggesting a 0.5 km grid spacing was required to simulate these fine-scale features. The large area of upward motion 0.25 to 1 m/s SW of Ellenville seen in Fig. 10 is consistent with the location and magnitude of the climb of WH in the 1st-wave region (1.1 m/s, Table 1).

The gravity-wave structure is shown well in the corresponding air motion simulations at the 700 and 500 mb level (Figs. 12 and 13, respectively). The WH climb in the 2nd-wave region from about 1800 to 1850 UTC, from about 2,000 m to 4,000 m MSL (through 700 mb), was just to the SW of PIO. Figure 12, which is similar to the 700 mb vertical motion field simulated for 1830 UTC, shows a band of w > 0.25 m/s across this region with nearby w > 0.5 m/s (at 850 mb there are patches of w > 1.0 m/s in this region during 1800 to 1845 UTC). Thus, the simulated air motion is consistent with the location of the WH climb in the 2nd-wave region, but of smaller magnitude than the achieved ascent of between 1.7 and 2.3 m/s (Table 1). Further, comparing the wave pattern at 500 mb (Fig. 13) with the Grid 3 topography (Fig. 9),

it appears several of the main axes of sinking air were aligned along the major drainages from the Catskills.

Comparing the simulated air motions at the 850, 700 and 500 mb levels (Figs. 10, 12 and 13) reveals that the wave structure becomes less "busy" with increasing altitude. That is, the BL rolls break up the wave pattern at 850 mb. But, since the rolls do not reach 700 mb, the wave structure is less broken up and more continuous. However, the deep wave structure at 700 mb is "busier" than at 500 mb. The vertical cross-sections, to be discussed, show how multiple waves of relatively narrow width formed between the surface and 700 mb merged into fewer waves of broader width by 500 mb.

The final ascent region of WH to almost 500 mb occurred about 12 km to the WNW of PIO from about 1915 to 2030 UTC. Figure 14 reveals the simulated wave pattern at 500 mb at 1930 UTC. It can be seen, the ascent is in a wave of w > 0.25 m/s (at 700 mb, the wave region had w > 0.5 m/s during this period). Vertical motion was stronger at 500 mb earlier in this region (Fig. 13), so WH could have encountered stronger lift had it managed to arrive in the region earlier.

Vertical cross-section views of the simulations

The south-to-north cross-section though the 1st-wave region just SW of ELN is depicted on Grid 3 at about y = -4 km in Fig. 15. The region of rising air (w > 0.5 m/s) extends from near the surface through 1,500 m MSL (about 850 mb). The area of rising air, which is also seen in the plan-view in Fig. 10, is consistent with the climb of WH in the 1st-wave region (1.1 m/s, Table 1).

The south-to-north and the east-to-west cross-sections at 1830 UTC through the 2nd-wave region just SW of PIO are depicted, respectively, on Grid 4 in Figs. 16 and 17. The region is at about y = 12.5 km in Fig. 16 and x = 12 km in Fig. 17. Both cross-sections show the region of w > 0.5 m/s to extend to about 3,000 m MSL and w > 0.25 m/s to about 4,000 m MSL. In the region, WH reached near 4,000 m MSL at 1850 UTC (Fig. 2) achieving 1.7 to 2.3 m/s climb rates (Table 1). Thus, the location of the 2nd wave-ascent region was accurately simulated but the vertical air speed was smaller than that achieved by WH (especially if the 0.6 m/s sink rate of WH is added to the achieved climb rate to estimate the actual vertical air speed).

The climb in the 3rd-wave region was made just NW of PIO (Fig. 1) and immediately north of the 2nd-wave region. There WH reached 15,500 ft MSL (4,700 m MSL, Fig. 2) at 1910 UTC with a climb rate of 1.2 m/s. The cross-sections (not shown) with the same coordinates as Figs. 16 and 17 but for 1915 UTC revealed an air motion pattern similar to that illustrated in Figs. 16 and 17. No rising air is apparent in Figures 16 and 17 that would allow WH to reach 4,700 m MSL. Thus, the simulation appears to have missed the 3rd-wave region.

The south-to-north and the east-to-west cross-sections at 2000 UTC through the 4th-wave region WNW of PIO are depicted, respectively, in Figs. 18 and 19. The region is at about y = 18.5 km in Fig 18 and x = 5 km in Fig 19. Both cross-sections show a region of w > 0.5 m/s to extend to about 5,400 m MSL. In the region, WH reached the high point of 5,483 m MSL at 2027 UTC (Fig. 2) achieving 1.4 m/s climb rate (Table 1). Thus, the location of the 4th wave-ascent region was accurately simulated and the air motions were similar in magnitude to those achieved by WH. However, if the 0.6 m/s sink rate of WH were added to the

achieved climb rate of 1.4 m/s to estimate the true vertical air speed, then the simulation underestimated the actual vertical air speed. From the simulation, it appears WH could not have climbed much higher in the 4th wave region. However, as seen in Fig. 18, if WH had been successful in the NW penetration after leaving the 4th wave region and contacted the base of the wave region at about y = 42 km, WH may have been able to climb to about 8500 m MSL! This conclusion is based on cross-sections extending to model top (not shown).

Discussion

The 1-D model analyses produced results consistent with the 2nd, 3rd and 4th wave regions encountered by WH but did not reproduce the 1st wave region. The 1st wave region was just upwind of the significant ridge east of the Ellenville Airport. And, the two-mountain simulation did not reproduce the 1st wave region either. Perhaps the first wave, being the primary, was not a trapped wave as the linear model being used assumes. The Lyra-Scorer parameter values are plotted against altitude in Fig. 8. It can be seen that the values are negative in the convective boundary layer and increase sharply at the boundary with the stable layer above. Thereafter, the values decreased almost monotonically with altitude. The sharp decreases at about 12,000 and 18,000 ft triggered waves in the algorithm. However, the general decrease in the parameter in the stable layer suggests waves were generated throughout the layer as the flight of WH defined. According to the 1-D model results, the 1st wave region was not explained but it appears WH may have been able to climb to almost 19,000 ft (5,800 m) MSL in the 4th wave region had clearance been obtained.

Remarkably, the extremely high-resolution (time and space) RAMS simulations reproduced much of the atmospheric conditions consistent with the well-documented mountain wave flight. The "checkerboard" cloud pattern revealed in satellite images was reproduced in the air motion simulation. The cloud pattern also was reproduced in the corresponding simulated relative humidity field. Thus, this extraordinary mountain wave appears to have been launched by convective activity in the form of boundary layer rolls within the boundary layer above the Catskill Mountains. Further, the large area of upward motion SW of Ellenville seen in the plan- and cross-section simulations is consistent with the location and magnitude of the climb of WH in the 1st-wave region. The simulated air motions are consistent with the location of the WH climb in the 2nd-wave region, but the amplitude is a smaller that the achieved ascent. The simulations appear to have missed the 3rd-wave region. The location of the 4th-wave region was accurate but the simulated air motions were weaker than those achieved by WH. From the simulation, it appears WH could not have climbed much higher in the 4th-wave region. However, if WH had been successful in the NW penetration after leaving the 4th region and contacted the base of the next wave region, WH may have been able to climb to about 8,500 m MSL!

The evolution of the BL rolls is clearly evident in the 0.5 km grid-spacing plan-views simulations and the depth of the BL rolls is clearly illustrated in the cross-sections. They appear to reach 1,500 m MSL, approximately the 850 mb level. Additionally,

the rolls were confined to the mountains indicating their presence amplified the wave structure described by Worthington[4]. Such rolls were not reported in the recent extraordinary measurements and numerical simulations of mountain waves in the Alps by Volkert, et al.[10] and Doyle and Smith[11]. Current knowledge of the rolls has been summarized by Young, et al.[12]. At the Congress, similar "checkerboard" could patterns were reported to have been flown in the Appalachians of the USA by M. Maughmer (where there are called "city streets") and in Germany by G. Waibel.

Conclusions

On 5 July 2002, a glider (WH) climbed to 17,990 ft MSL (5,485 m MSL) in a mountain wave over the Catskill Mountains of NY State USA. According to the 1-D numerical model simulation of the event, the 2nd, 3rd and 4th-wave regions encountered by WH were explained and it appears WH may have been able to climb to almost 19,000 ft MSL in the 4th-wave region had clearance been obtained.

From the RAMS simulation of the event, the locations of the 1st, 2nd and 4th-wave regions encountered by WH were reproduced, though, the magnitudes of the simulated vertical air motions were underestimated. It appears from the simulations that WH could not have climbed much higher in the 4th-wave region. However, if WH had been successful in the NW penetration after leaving the 4th-wave region and contacted the base of the next wave region, WH may have been able to climb to about 8,500 m MSL!

The evolution and depth of the convective boundary rolls that were confined to the Catskill Mountains were clearly illustrated in RAMS simulations and were implicit in the 1-D simulations. Thus, this extraordinary mountain wave appears to have been enhanced by convective activity within the boundary layer above the Catskill Mountains.

The success of the RAMS in reproducing the atmospheric conditions during the remarkable flight of WH indicates the model can be used to forecast wave conditions for other soaring flights.

Acknowledgements

References

[1]Barone, G., Personal communication, (2003).

[2]Durran, D. R., Mountain waves, In *Mesoscale Meteorology and Forecasting*, P. S. Ray, editor, Am. Meteor. Soc., Boston, 472-492, (1986).

[3]Worthington, R. M., Lenticular wave cloud above the convective boundary layer of the Rocky Mountains. *Weather*, **57**, 87-90, (2002).

[4]Worthington, R. M., Mountain waves launched by convective activity within the boundary layer above mountains. *Boundary-Layer Meteorology*, **103**, 469-491, (2002).

Worthington, R. M., Convective mountain waves above Cross Fell, northern England. *Weather*, **60**, 43-44, (2005).

[5]Bradbury, T. A. M., Links between convection and waves. *Meteorol. Mag.*, **119**, 112-120, (1990).

[6]Schewchuck, J. D., *RAOB Users Guide*. Environmental Research Services, 1134 Delaware Dr., Matamoras, PA USA 18336-9708, (1997), www.raob.com.

[7]Corby, G. A. and C. E. Wallington, Airflow over mountains: The lee-wave amplitude. *Quart. J. Royal Meteor. Soc.*, **82**, (1956).

[8]Cotton, W. R., et al., RAMS 2001: Current status and future directions. *Meteor. and Atmos. Physics*, **82**, 5-29 (2003).

[9]Cotton, W. R., G. Thompson and P.W. Mielke, Real-time mesoscale prediction on workstations. *Bull. Amer. Meteor. Soc.*, **75**, 349-362, (1994).

[10]Volkert, H., C. Keil, C. Kiemle, G. Poberaj, J.-P. Chaboureau and E. Richard, Gravity waves over the eastern Alps: A synopsis of the 25 October 1999 event combining *in situ* and remote-sensing measurements with a high-resolution simulation. *Quart. J. Royal. Meteor. Soc.* **129**, 777-797 (2003).

[11]Doyle, J. and R. Smith, Mountain waves over the Hone Tauern: Influence of upstream diabatic effects. *Quart. J. Royal. Meteor. Soc.* **129**, 799-823 (2003).

[12]Young, G., D. Kristovich, M. Hjelmfelt and R. Foster, Rolls, streets, waves and more: A review of quasi-two-dimensional structures in the atmospheric boundary layer. *Bull. Am. Meteor. Soc.*, **83**, 997-1001 (2002).
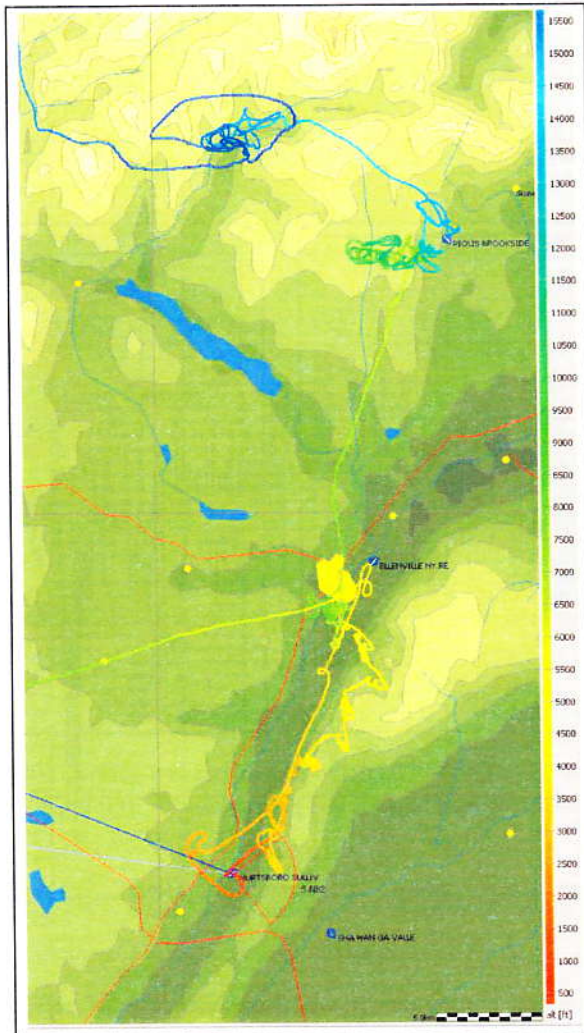
Figure 1. The flight track of WH superimposed on the topography. The color wedge on the right corresponds to altitudes in feet MSL. The horizontal scale at the bottom is 5 km in length.
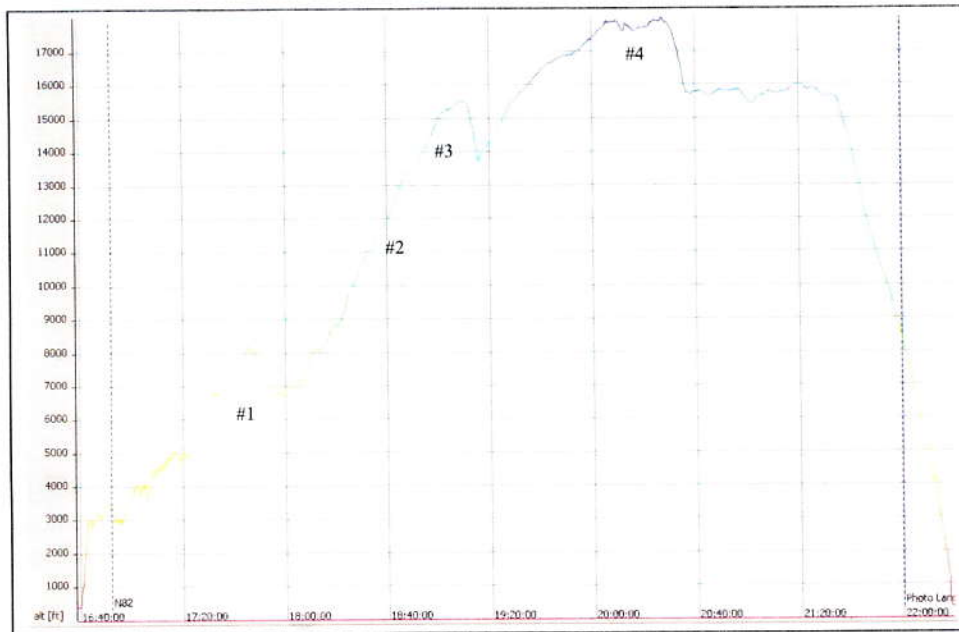

Figure 2. The barogram trace of WH. The abscissa is time (UTC) and the ordinate is altitude (feet MSL). The four climb regions are indicated.
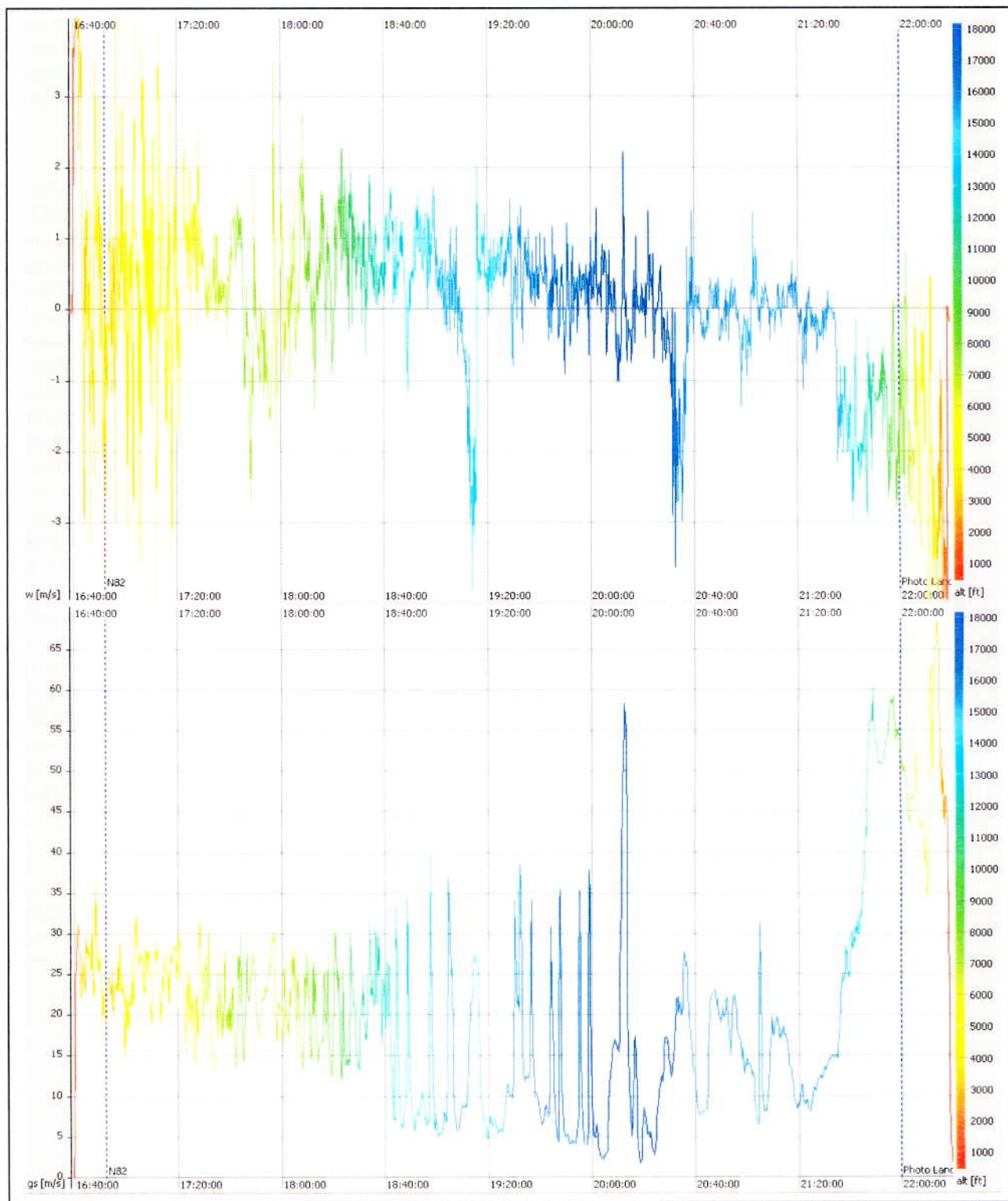
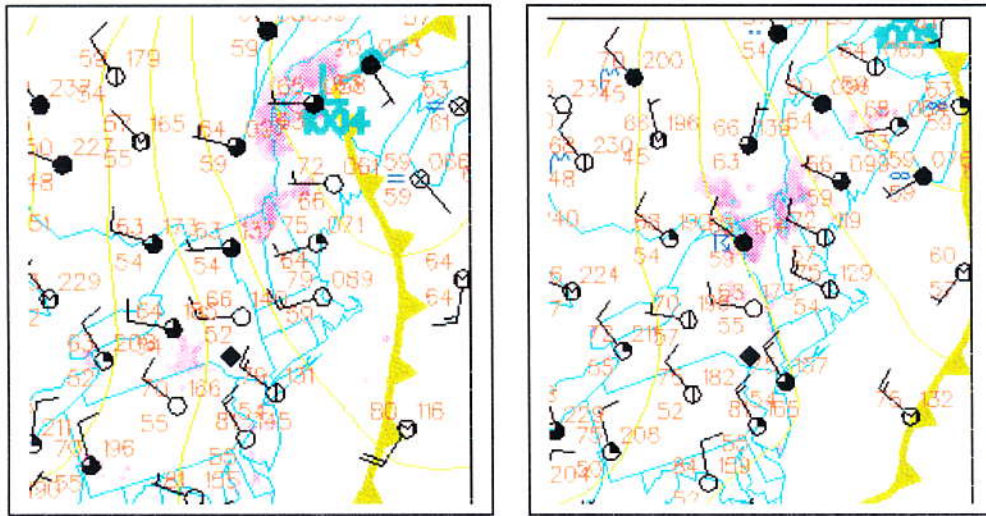**Figure 3**. Upper: The variometer trace of WH (+/-4 m/s full scale) vs time (UTC). Lower: The corresponding GPS ground speed trace (0-65 m/s full scale) vs time (UTC).

Figure 4. 5 July 2002 surface weather map for (left) 0700 EST (12UTC) and (right) 1900 EST (00UTC, 6 Jul 03). Wurtsboro, NY is located near the diamond shape.
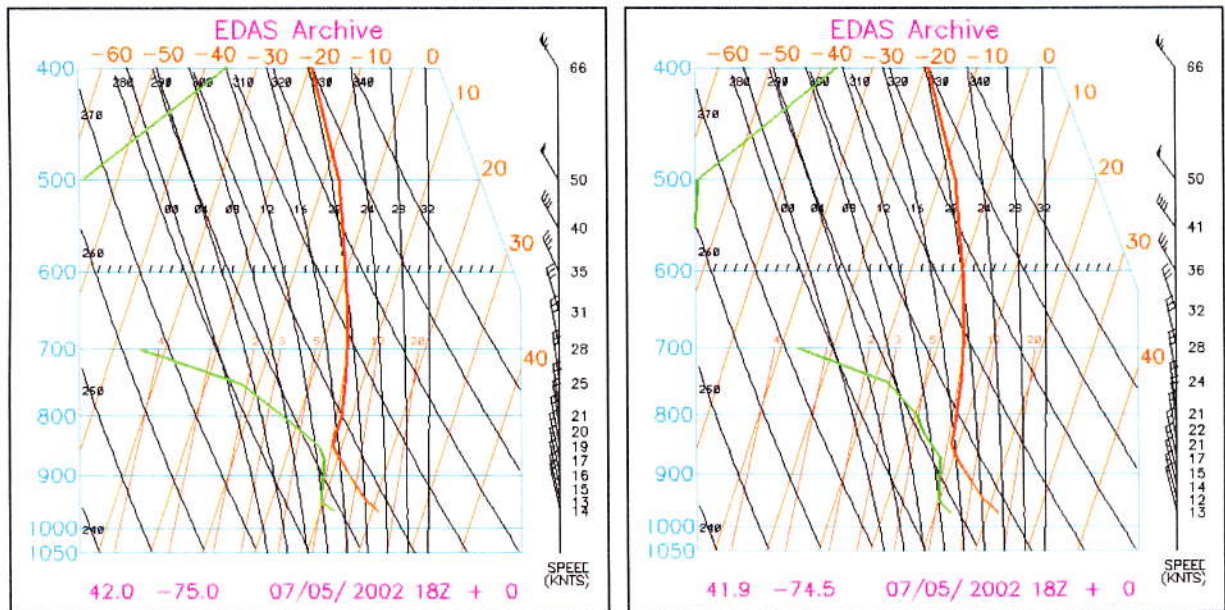
Figure 5. The 18 UTC (1300EST) soundings during the wave flight of 5 July 2002. Left: the upwind sounding near Oneonta, NY. Right: the sounding over Piolis Ariport. Note the temperatures are in C and the pressures are in mb (from www.arl.noaa.gov/ready/amet.html)
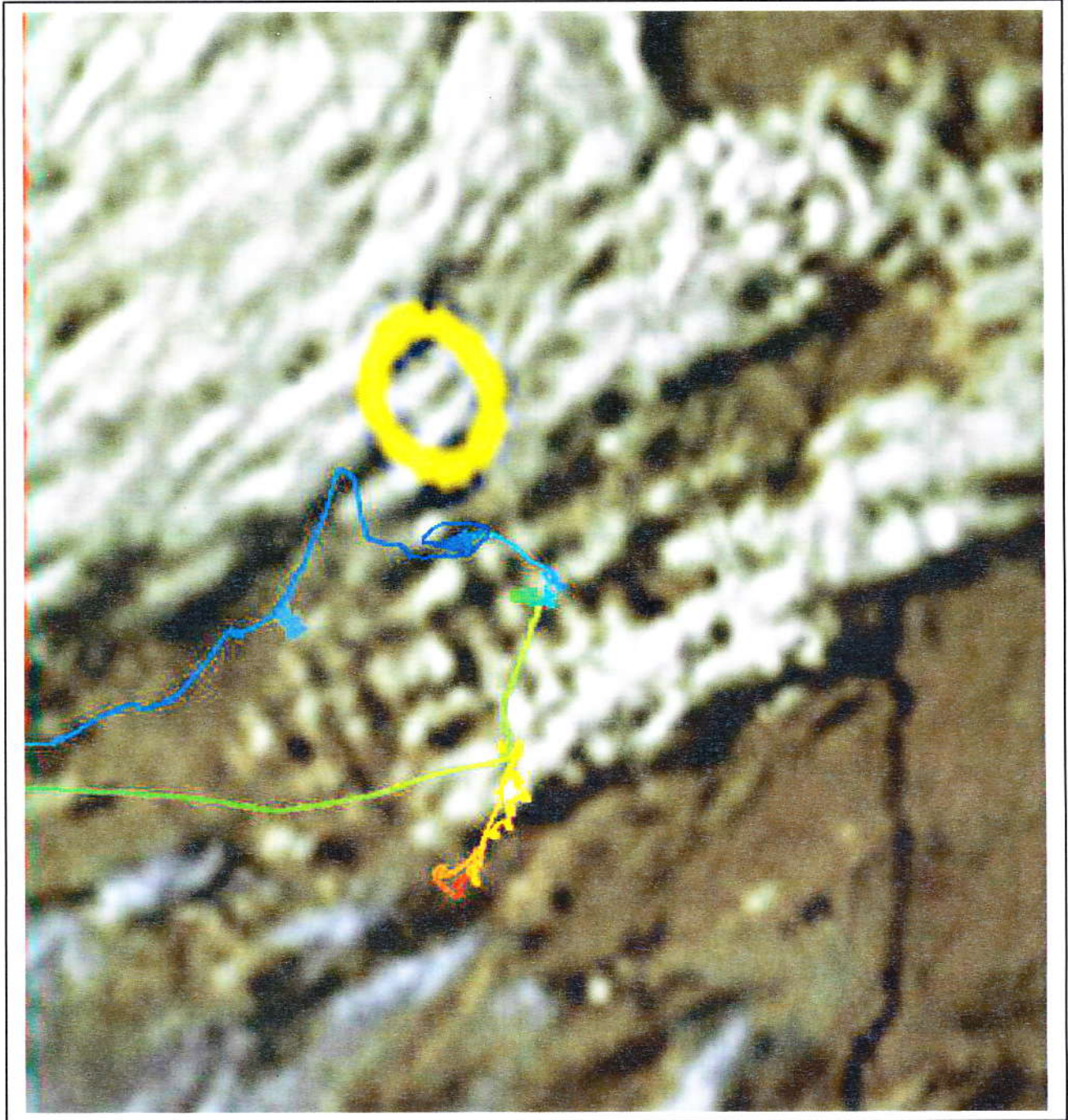
Figure 6. The 2225 UCT (1725 EST) NOAA14 visible image obtained following Worthington[3] using software from www.david-taylor.pwp.blueyonder.co.uk/software/hrpt.htm. The large yellow circle surrounds 42.2N, 74.5W and the N-S oriented Hudson River can be seen in the lower right of the image. The track of WH is the line that changes colors: the warm colors are low altitudes (500 ft) while the cold colors are high altitudes (18,000 ft).
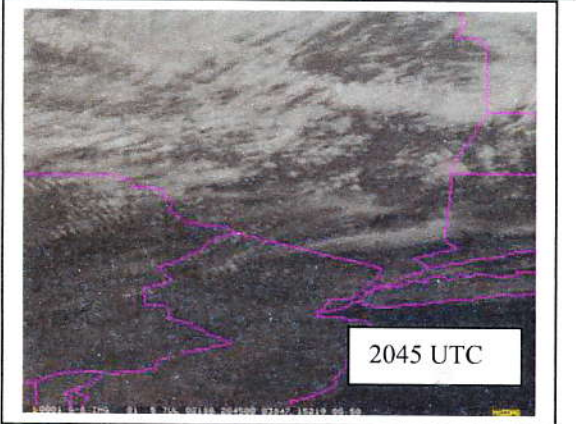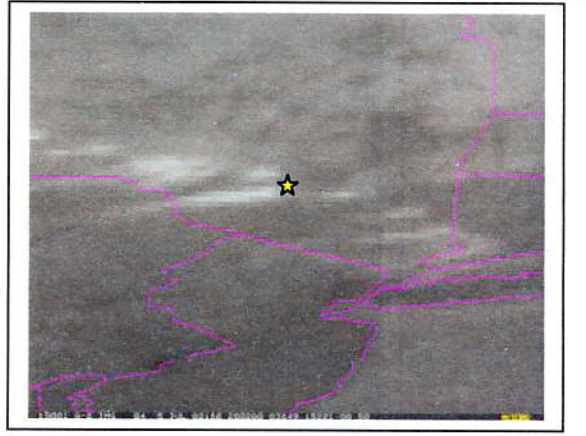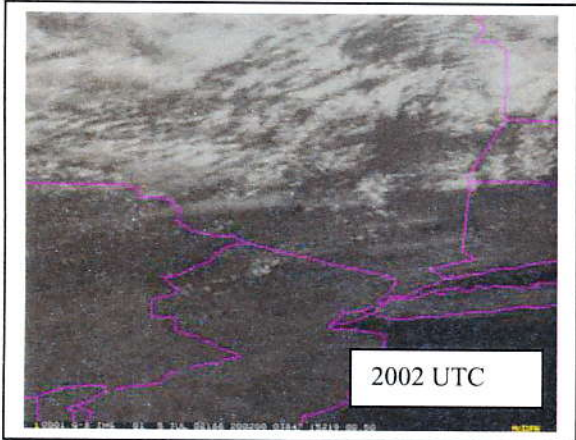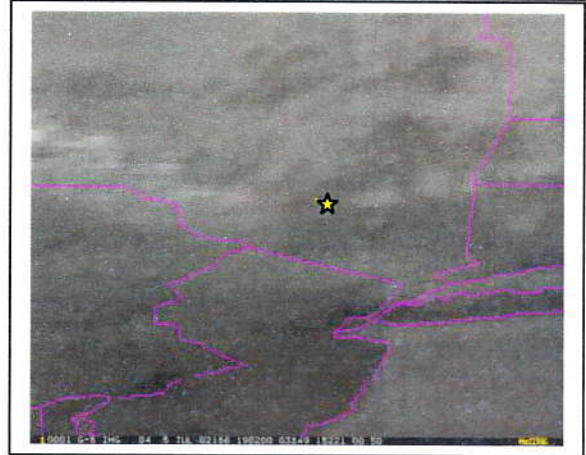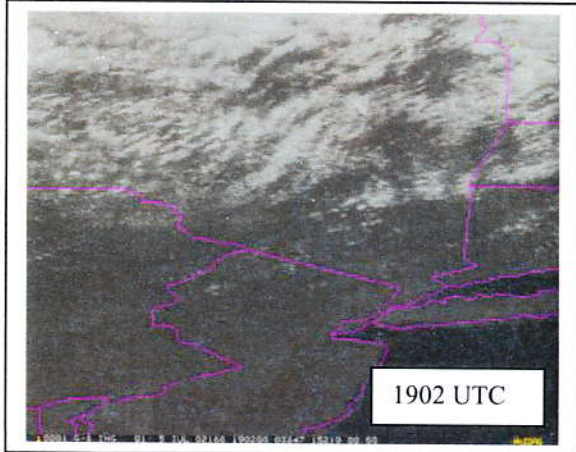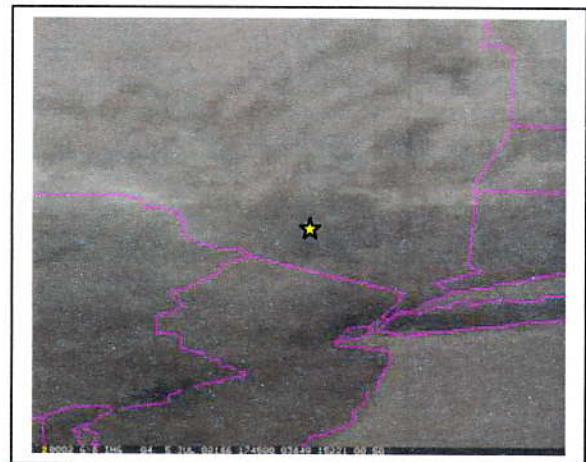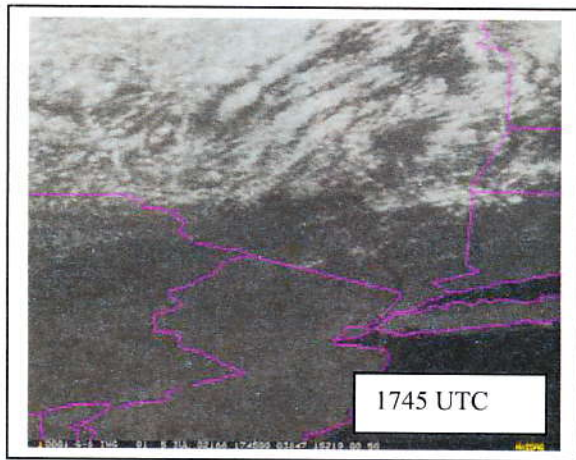
Figure 7. Pairs of visible (left) and infrared (right) GOES-EAST images for 5 July 2002. The location of WH is marked by a yellow symbol near the center of each infrared image.
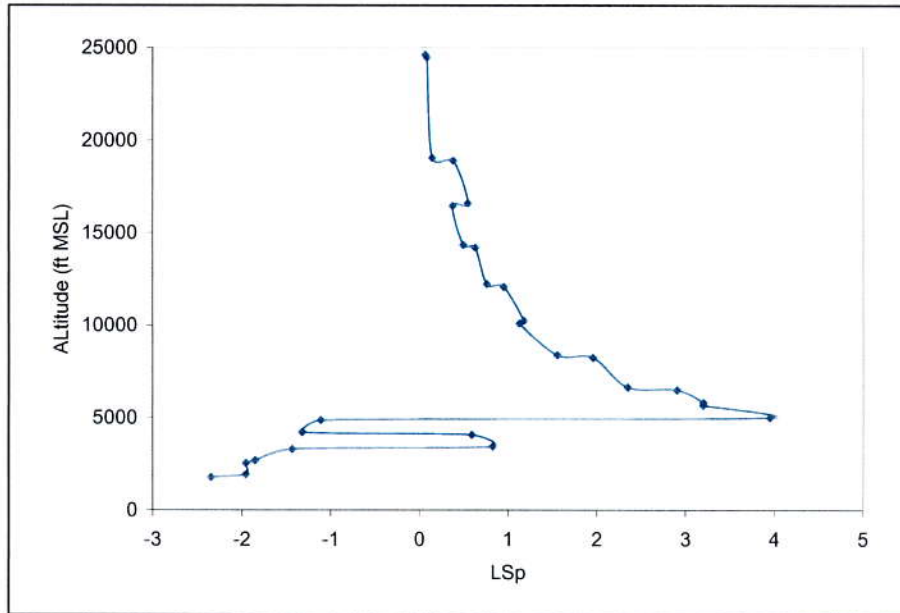
Figure 8. The Lyra-Scorer parameter (LSp, m^{-2}) for the upwind sounding near Oneonta, NY displayed in Figure 5.
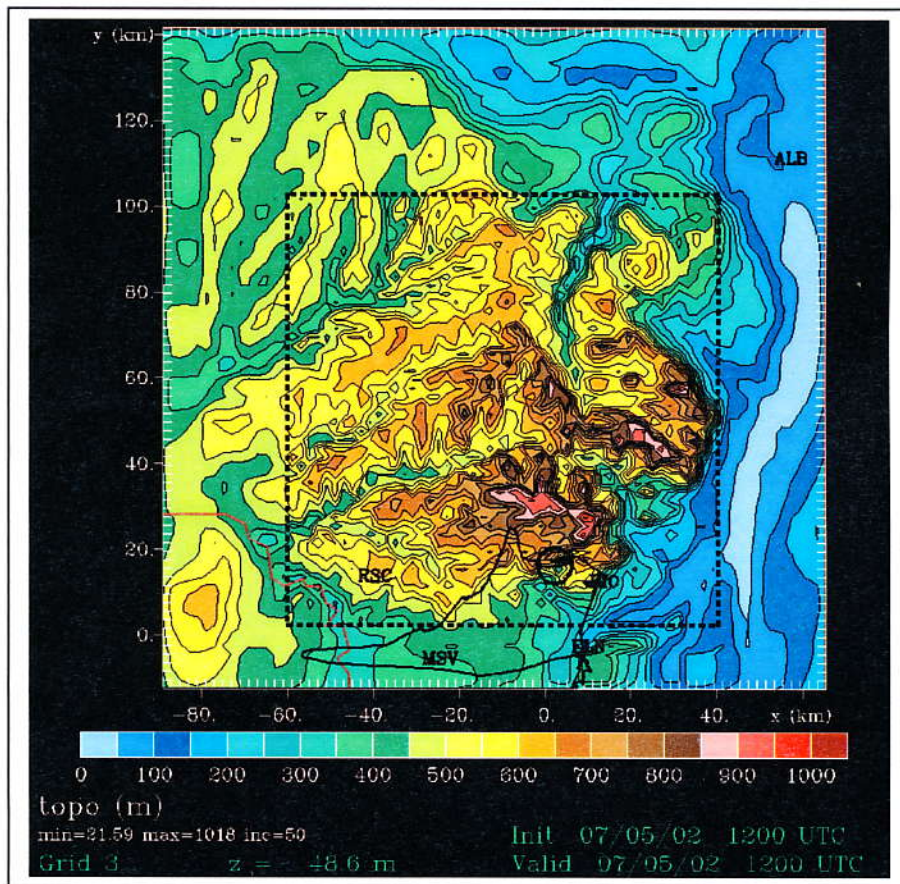
Figure 9. RAMS Grid 3 (2 km grid-point spacing) is the outer grid and Grid 4 (0.5 km grid-pint spacing) is the inner grid. The locations of Ellenville (ELN), Pilois (PIO), Monticello/Sullivan (MSV), Rosco (RSC) and Albany (ALB) New York airports are indicated. The WH flight track is the continuous black line. The circle is the region of highest climb.
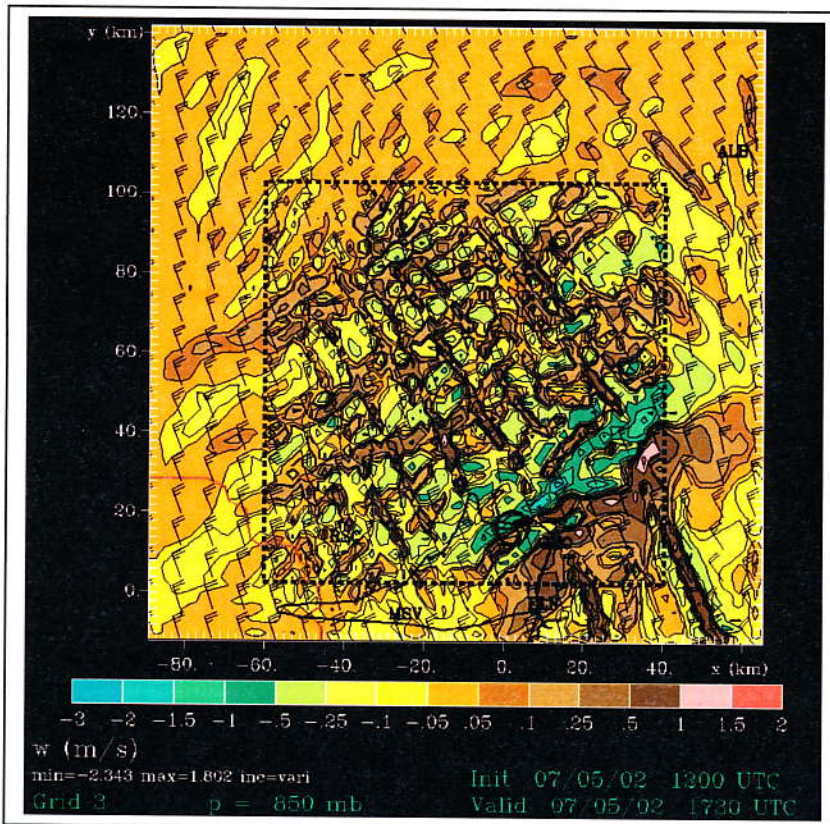
Figure 10. Simulated air flow at 850 mb for 1730 UTC on Grids 3 and 4. The vertical motion field is colored. The horizontal motion is indicated by the wind barbs: flag, barb and half-barb = 25, 5 and 2.5 m/s (about 50, 10 and 5 kt).
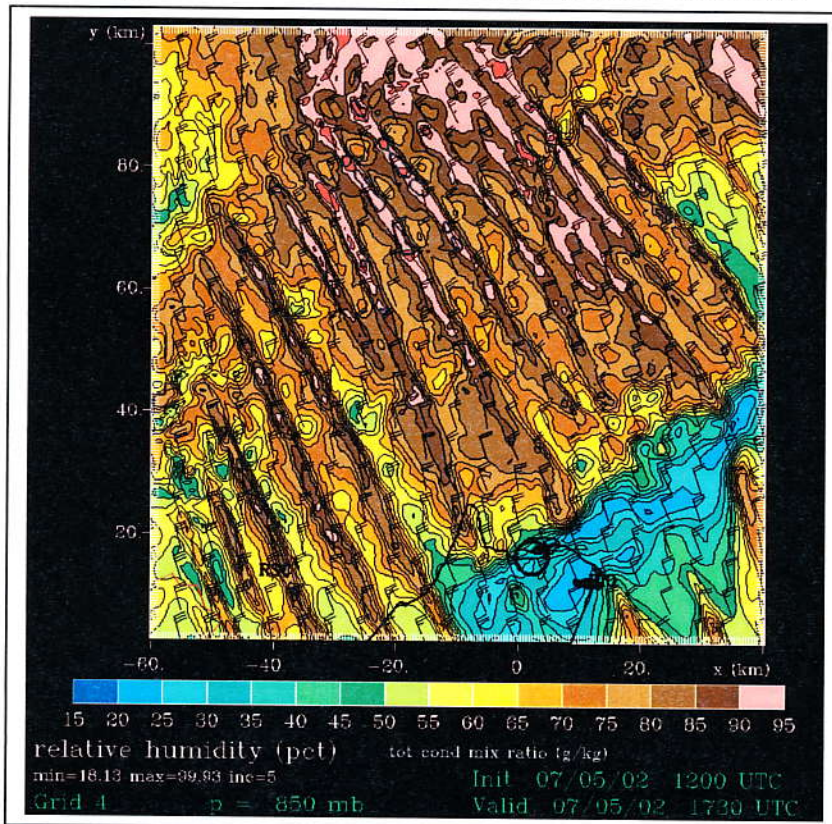
Figure 11. Simulated relativity humidity at 850 mb for 1730 UTC on Grid 4. Regions of red are cloud; the black contours in the BL rolls are regions with total condensate mixing ratios ≥ 0.01 g/kg.
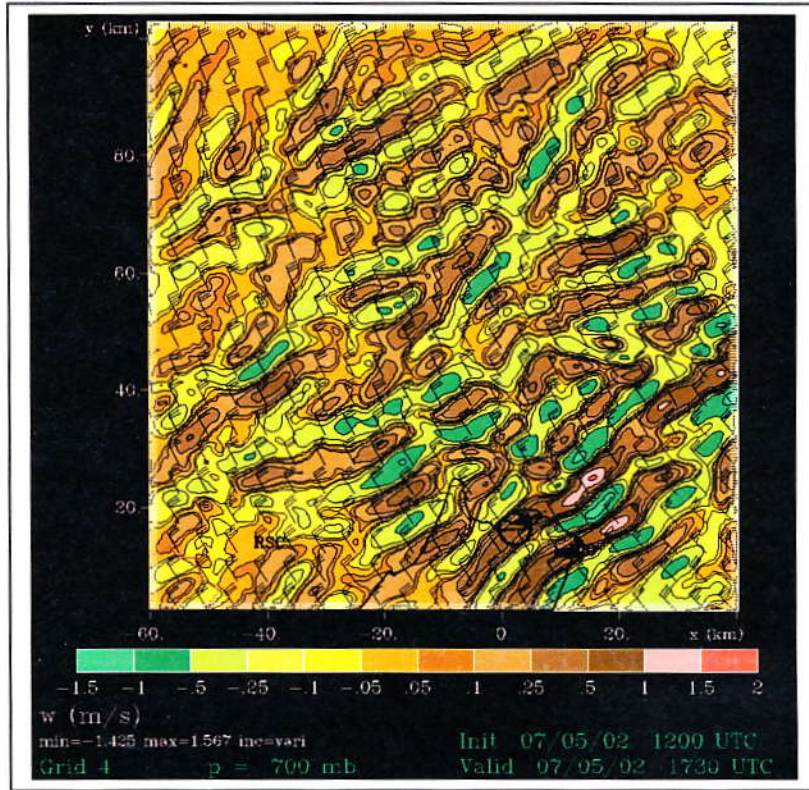
Figure 12. Simulated air flow at 700 mb for 1730 UTC on Grid 4.
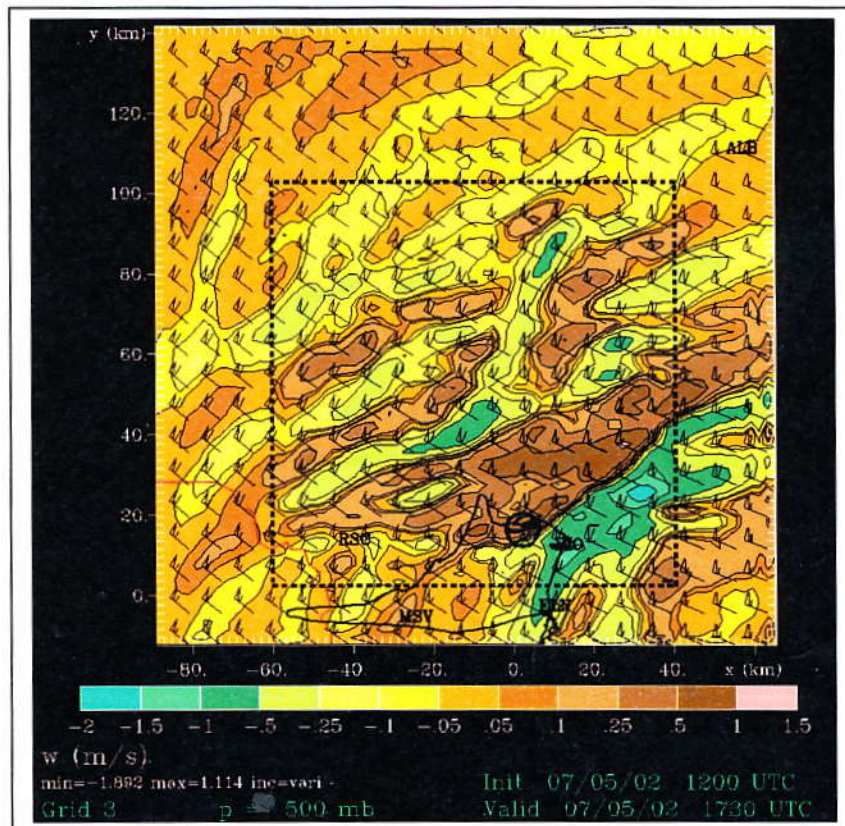
Figure 13. Simulated air flow at 500 mb for 1730 UTC on Grids 3 and 4.
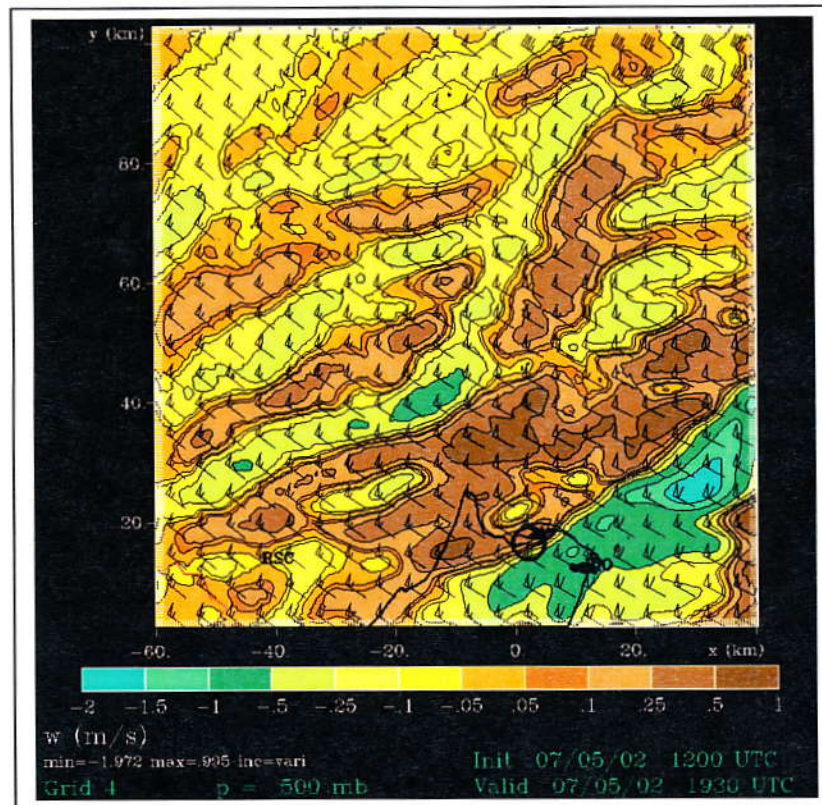
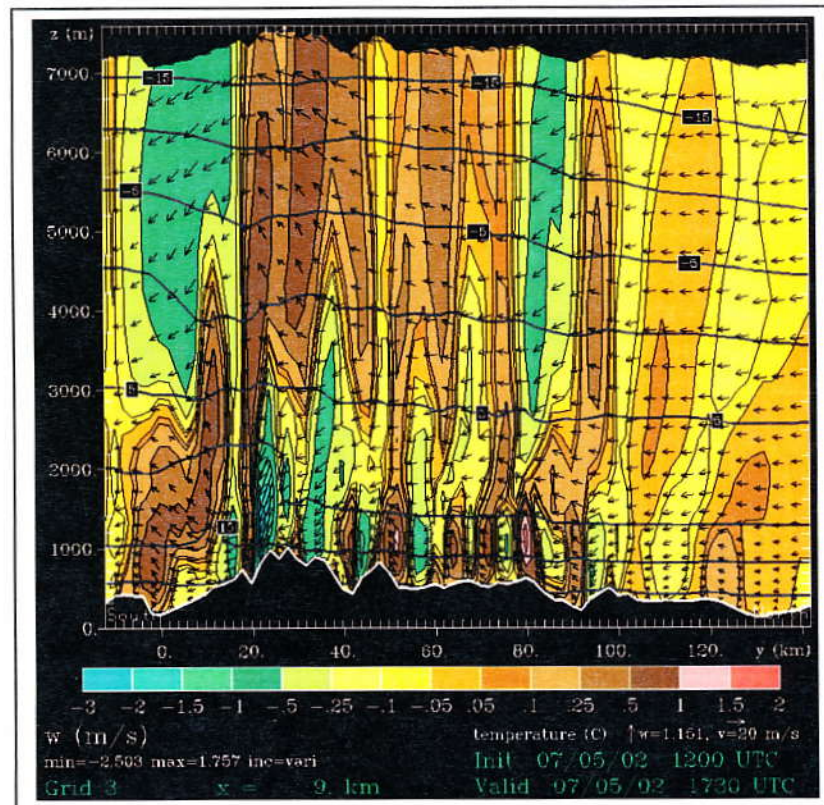**Figure 14**. Simulated air flow at 500 mb for 1930 UTC on Grid 4.

Figure 15. South-to-north cross-section at 1730 UTC through x = 9 km (74.39W) on Grid 3. The vertical motion field is colored. The vectors define the u and w components of the airflow (scale in lower right corner). Black temperature contours are at 5C intervals.
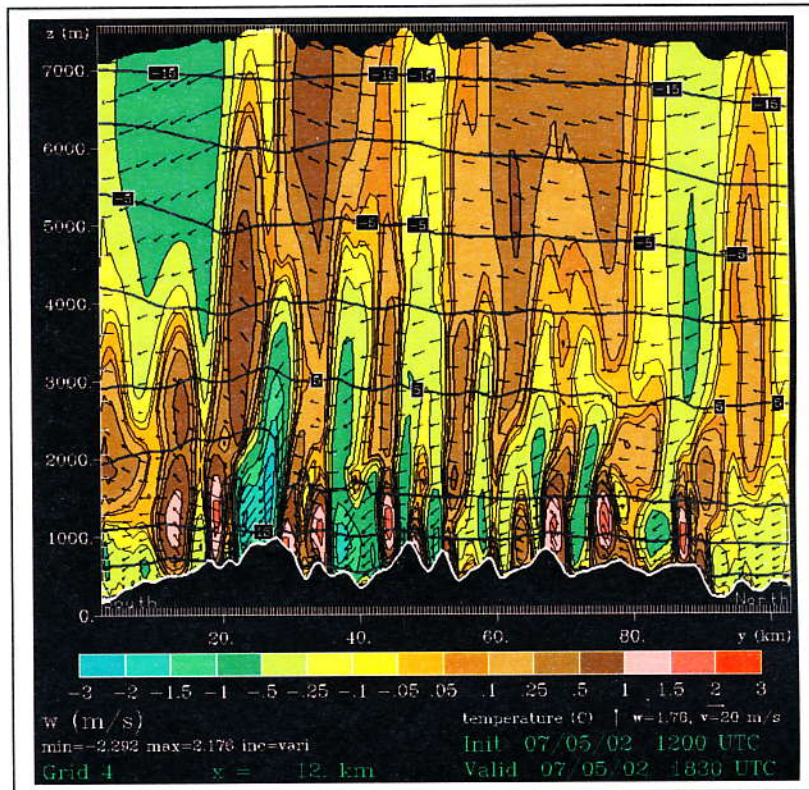
Figure 16. South-to-north cross-section at 1830 UTC through x = 12 km (74.36W) on Grid 4. The wind components and temperature contours are as in Fig. 15.
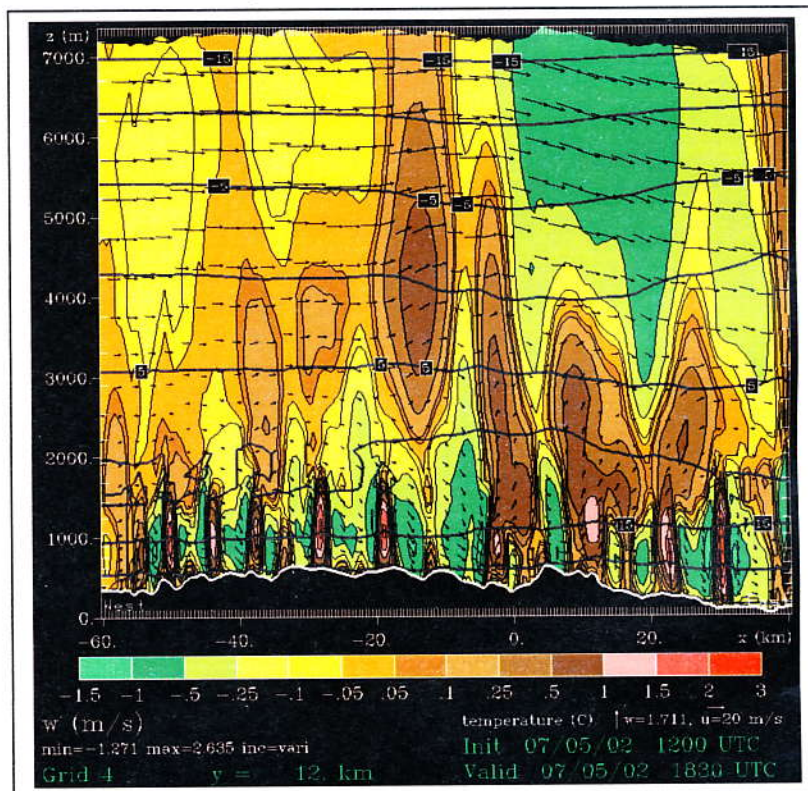

Figure 17. West-to-east cross-section at 1830 UTC through y = 12.5 km (41.86N) on Grid 4. Note, the 0.5 of the coordinate y = 12.5 does not get included in the information below the plot. The vertical motion field and temperature contours are as in Fig. 15 and the wind components are u/w.
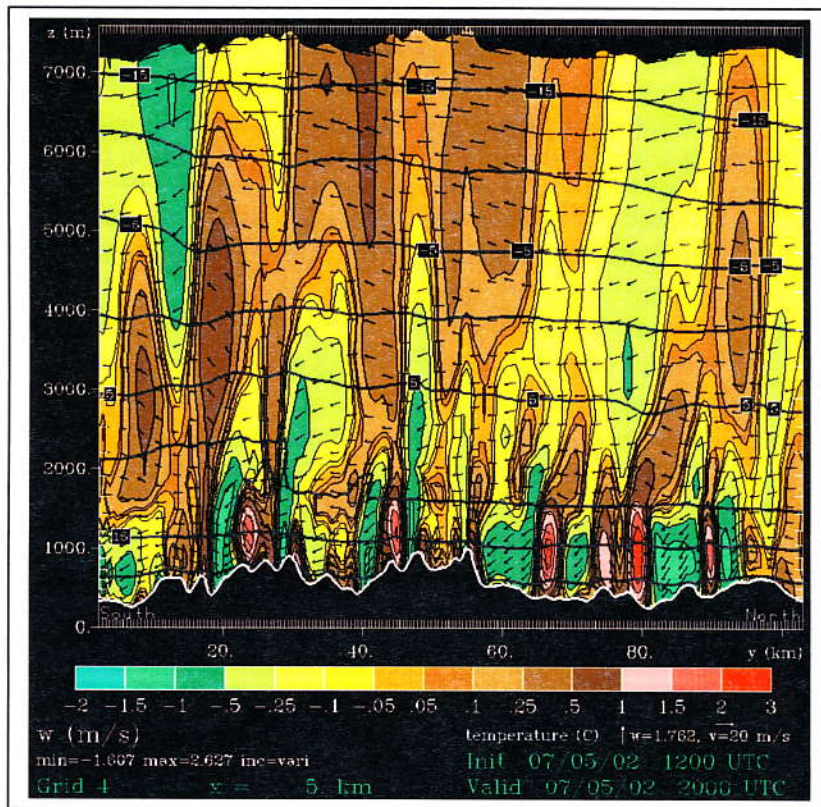
Figure 18. South-to-north cross-section at 2000 UTC through x = 5 km (74.44W) on Grid 4. The wind components and temperature contours are as in Fig. 15.
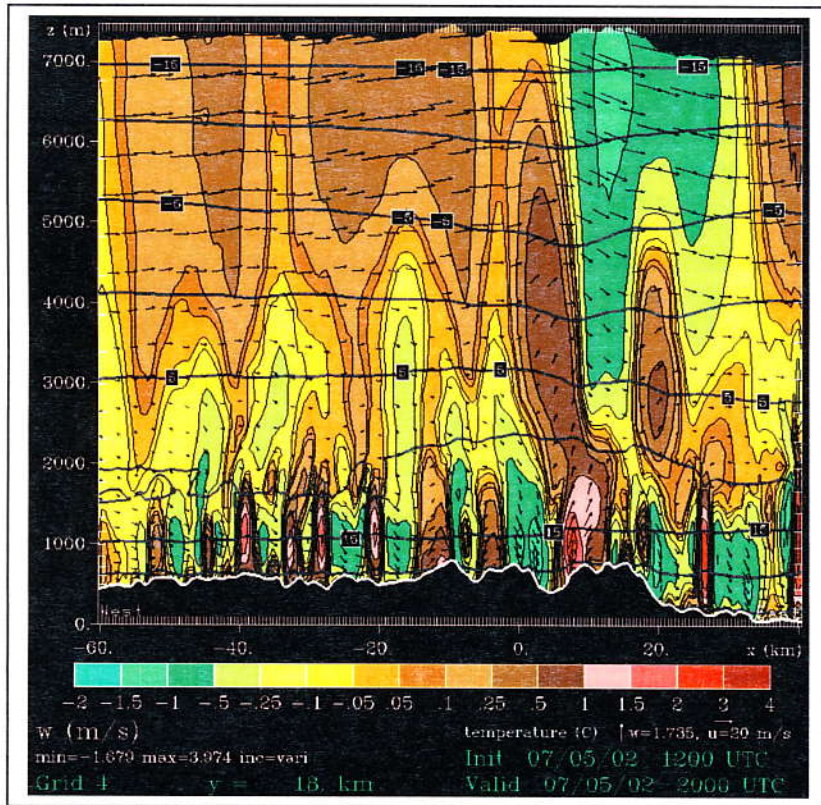

Figure 19. West-to-east cross-section at 2000 UTC through y = 18.5 km (41.92N) on Grid 4. The vertical motion field and temperature contours are as in Fig. 15 and the wind components are u/w.

Table 1					
Wind estimates from WH GPS flight track data					
(Note, it was not possible to estimate wind direction in wave)					
Time (UTC)	Lift source	Altitude band (ft MSL)	Horiz. wind (m/s)	Wind direction (degrees true)	Vert. wind (m/s)
16:45	thermal	3000-5000	10.5	337	2.4
16:49	thermal	3200-3600	9.7	332	2.1
17:05	thermal	4000-4300	8.6	334	2.3
17:27	1st wave	6000-6400	5	-	1.1
18:02	2nd wave	6900	5	-	1.7
18:20	2nd wave	8000-9000	9	-	2.3
19:02	3rd wave	15,187	14	-	1.2
20:02	4th wave	17,600	12	-	1.4